JOURNAL OF MATERIALS SCIENCE 25 (1990) 3641–3648

Sintering process of Y_2O_3-added Si_3N_4

OSAMI ABE
Government Industrial Research Institute, 1-1 Hirate-cho, Kita-ku, Nagoya 462 Japan

The sintering process of Y_2O_3-added Si_3N_4 has been investigated by dilatometry and microstructural observations. Densification was promoted above 1440° C by the formation of eutectic melts in the Y_2O_3–SiO_2–Si_3N_4 triangle. However, the dilatometric curves indicated no shrinkage corresponding to the rearrangement process, despite liquid-phase sintering. The kinetic order for the initial-stage sintering was 0.47 to 0.49. These values indicated that the phase-boundary reaction was rate controlling. The apparent activation energy (323 kJ mol^{-1}) was smaller than the dissociation energy for the Si–N bond (435 kJ mol^{-1}). ESR data and lattice strain indicated that the disordered crystalline structure of the Si_3N_4 starting powder promoted the reaction of Si_3N_4 with eutectic melts. After a period of initial-stage sintering, the formation of fibrous β-Si_3N_4 grains resulted in interlocked structures to interrupt the densification.

1. Introduction

Silicon nitride ceramics are expected to be high-temperature structural materials because of their high strength and high fracture toughness [1, 2]. The high fracture toughness is attained by the twinned fibrous grains formed in the sintered bodies during liquid-phase sintering [3]. However, the glassy grain boundary phases degrade strength at elevated temperatures [4, 5]. On the other hand, when preparing sintered bodies with only a small amount of glassy phases by solid-state reaction sintering [6] or hot isostatic pressing (HIP) without oxide additives [7], the resulting equiaxial grains considerably degrade the fracture toughness. Therefore the sintering process must be further optimized according to kinetic information for grain growth and densification.

Many studies have been carried out on the kinetics of densification and α/β transformation of Si_3N_4 [8–17]. However, some processes in kinetics and reactions have not been yet clarified. For example, Hampshire and Jack [10] have shown that the densification of Y_2O_3-added Si_3N_4 progressed through a diffusion-rate-controlling sintering after a rearrangement process. Instead, Babini *et al.* [17] have suggested a boundary-reaction rate-controlling mechanism for the hot presssing of Y_2O_3–Si_3N_4–SiO_2 system, where the solution of Si_3N_4 into the melts was the rate-determining step. Such contradictions, which can also be found in studies of MgO-added Si_3N_4 [8, 10, 11], require precise measurements of shrinking behaviour. Therefore in this study shrinkage and shrinking rate of Y_2O_3-added Si_3N_4 were measured precisely by using a specially assembled high-temperature dilatometer. Kinetic parameters were discussed in relation to the microstructure.

2. Experimental procedure

2.1. Materials

High-purity α-Si_3N_4 powder (Denka Co. Ltd, Tokyo, grade SNGX) was used as a starting material. The metallic impurity (15 elements), oxygen content and specific surface area were 227 p.p.m., 1.02 wt % and 15.3 m^2 g^{-1}, respectively. This powder was synthesized by nitridation of silicon powder and consisted of irregularly shaped particles. Yttria powder (Hokko Chemicals Co. Ltd, Tokyo) with a specific surface area of 70.9 m^2 g^{-1} was used as a sintering aid. A powder mixture containing 6 mol % Y_2O_3 was prepared by wet mixing in methanol using a vibration ball mill. Drying was performed at 150° C under vacuum after evaporating the methanol at 80° C in a flow of N_2 gas (0.3 kPa). Mechanically prepressed green bodies (9 × 9 × 40 mm, 5 MPa) were isostatically pressed at 500 MPa. The green density was 1.94 ± 0.03 g cm^{-3}.

2.2. Equipment and procedure

The shrinking rate was measured by a high-temperature dilatometer as shown in Fig. 1. The maximum temperature and gas pressure applicable were 2300° C and 1.0 MPa, respectively. The shrinkage and shrinking rate of the samples and of a reference material (re-crystallized SiC, RCSC) were detected by transducers with a time resolution of 1 sec. To prevent the contamination of samples by carbon, most of the parts inside the heater were made of RCSC. The detection errors of shrinkage and shrinking rate were less than 1.78 × 10^{-2}% and 3.2 × 10^{-3}% min^{-1}, respectively. Details of the equipment have been discussed previously [18].

The temperature dependencies of shrinkage and shrinking rate were measured at 2 to 50 K min^{-1} in a N_2 atmosphere. Isothermal measurement was performed at a heating rate of 50 K min^{-1} at variable temperatures in the range 1525 to 1850° C. The applied load, gas pressure and gas-flow rate were 10 g, 1.0 MPa and 1.0 dm^3 min^{-1}, respectively.

The dilatometric measurements, bulk density and porosity were determined by Archimedes' principle. Microstructure was observed by scanning electron microscopy (SEM, JEOL JSM-T-33OAS). Grain-

0022–2461/90 $03.00 + .12

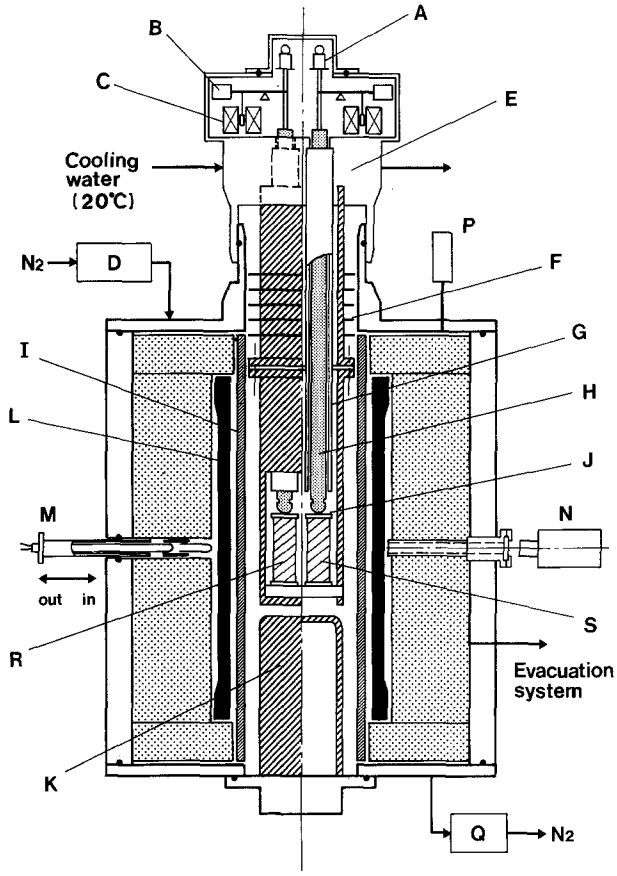

Figure 1 Inside view of high-temperature dilatometer, A, weight; B, counter-weight; C, transducer; D, gas-pressure controller; E, temperature-controlled block; F, radiation shield; G, sleeve; H, detector; I, shield tube; J, spacer; K, heat sink; L, heater; M, thermocouple (Pt–Rh); N, optical pyrometer; P, pressure gauge; Q, gas-flow-rate controller; R, reference; S, sample.

boundary phases were identified by X-ray diffractometry with Cu$K\alpha$ radiation (40 kV, 100 mA).

3. Results

3.1. Temperature dependence of shrinkage and shrinking rate

Figs 2 and 3 show the temperature dependence of shrinkage ($\Delta L/L_0$) and shrinking rate ($d(\Delta L/L_0)/dt\,v^{-1}$, v = heating rate), respectively. The dependence of commercially available Si_3N_4 (H.C. Starck, LC-12) was also measured for comparison. The final shrinkage in the transverse direction of the samples agreed well with the determined shrinkage in the lengthwise direction.

Figs 2 and 3 indicate that the densification progressed above the lowest eutectic temperature of the Y_2O_3–SiO_2–Si_3N_4 triangle (1440° C) [10]. The sinterability of the SNGX powder was somewhat improved compared with LC-12. However, the shrinkage corresponding to the rearrangement processes hardly appeared in spite of the liquid-phase sintering. The curves for the SNGX powder in both figures shifted toward higher temperatures with the increase in v. The final shrinkage at 1900° C decreased with decreasing heating rate because of the termination of shrinking at low temperatures. A slight expansion appeared around 1850° C at 2 to 10 K min^{-1}. The shrinking rate increased again above 1850° C at 2 and 5 K min^{-1} after expansion. The termination of densification was caused by the growth of fibrous grains as shown in Fig. 4. The body sintered at 2 K min^{-1} consisted of elongated large grains. The grain size was reduced with the increase in heating rate. The formation of the interlocked structures of large fibrous grains during sintering resulted in the termination of densification. The remarkably low shrinkage at 2 K min^{-1} could also be related to the thermal decomposition of the sample as described by Mitomo *et al.* [8], since the weight loss at 2 K min^{-1} was 7.34%, while it was less than 4.65% for the other samples.

3.2. Isothermal shrinkage and properties of heat-treated samples

Fig. 5 shows the isothermal shrinkage as a function of soaking time, t. The shrinkages at 1525 to 1750° C continuously increased with increasing soaking time. However, at 1850° C the shrinkage decreased for soaking times of 5 to 15 min and then slightly increased, as expected from Figs 2 and 3.

Fig. 6 shows the X-ray diffraction profiles of heat-treated samples. The α-Si_3N_4 contents are listed in Table I with other properties. At 1525 to 1600° C, $Y_2O_3 \cdot Si_3N_4$ (N-melilite) was only identified as the grain-boundary phase. The intensity of reflections for N-melilite weakened above 1700° C and disappeared at 1725° C. Reflections of $10Y_2O_3 \cdot 9SiO_2 \cdot Si_3N_4$

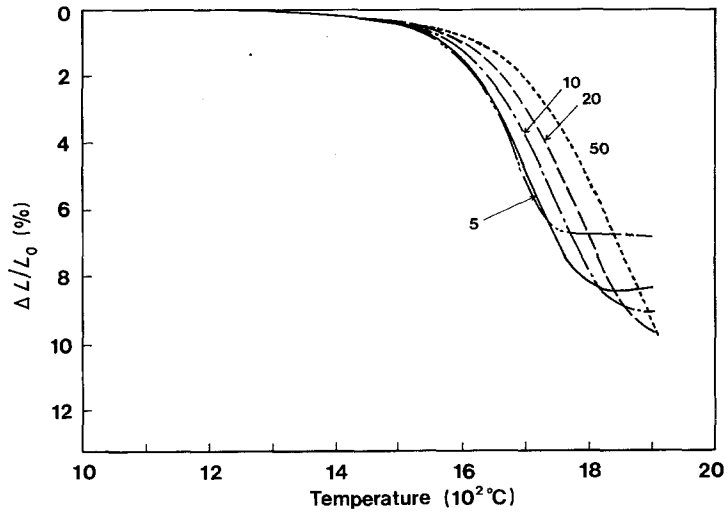

Figure 2 Temperature dependence of shrinkage ($\Delta L/L_0$). Heating rate, 2 K min^{-1}.

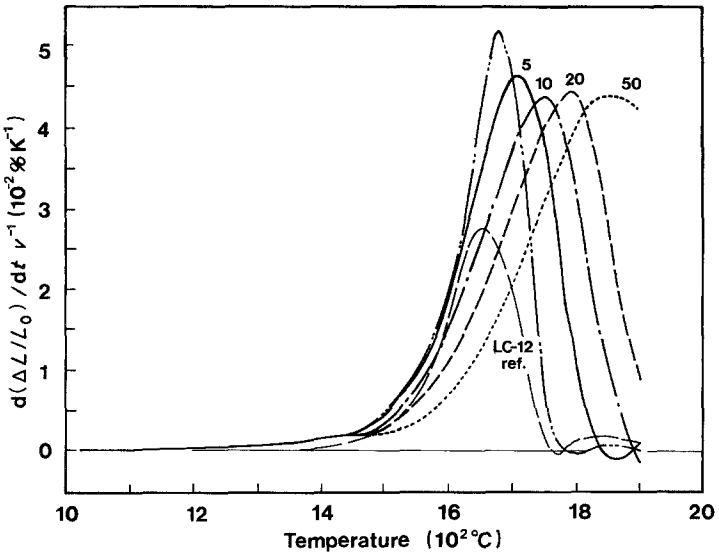

Figure 3 Temperature dependence of shrinkage rate divided by heating rate $[(\Delta L/L_0)/dt\,v^{-1}]$. $v = 2\,K\,min^{-1}$.

(N-apatite) appeared above 1650° C. Reflections similar to those of $4Y_2O_3 \cdot SiO_2 \cdot Si_3N_4$ (N-wohlerite) appeared at 1850° C. However, the formation of N-wohlerite was not reliable. Table I indicated that the α/β transformation was very slow at 1525 to 1600° C and was remarkably promoted above 1650° C.

The fracture surface of heat-treated samples is shown in Fig. 7. The small particles of less than 0.1 μm in the starting powder were consumed, and spherical or roundish grains with a smooth surface were formed at 1525 to 1600° C. The limited formation of fibrous grains below 1600° C agreed well with the slow transformation rate at that temperature range. At 1650 to 1675° C, the grains grew with the transformation. The aspect ratio was very small up to 1700° C. Fibrous grains were evidently developed above 1725° C (compare the microstructure at 1700° C with that at 1725° C).

3.3. Kinetic parameters

The microstructure shows spherical or roundish grains with low aspect ratio at 1525 to 1725° C. This satisfied the assumption in Kingery's model [19, 20] for application to the shrinking behaviour shown in Fig. 5. The kinetic order (n) in Kingery's expression, Equation 1 below, was obtained from the log–log plots shown in Fig. 8, assuming that the increase of r was negligible.

$$\Delta L/L_0 = kr^{-m}t_c^{-n} \quad (1)$$

where k is a kinetic constant, r = grain radius, t_c = corrected soaking time, and m, n are constants, where the soaking time (t) was corrected according to an approximately linear relation between t and log $(\Delta L/L_0)$ within 2 min after attaining the test temperatures. The shrinkage $(\Delta L/L_0)$ was not corrected, since the shrinkage of rearrangement process was negligibly small as shown in Figs 2 and 3.

The kinetic order (n) listed in Table I was 0.47 to 0.49 at 1525 to 1625° C. These values were close to the 0.50 expected for the boundary-reaction-controlling mechansim for spherical grains. The kinetic constant (k) in Equation 1 was obtained by plotting $\Delta L/L_0$ against $t^{-0.5}$. The activation energy obtained from the Arrhenius plot shown in Fig. 9 was 323 kJ mol^{-1}.

4. Discussion

4.1. Densification process

The densification took place without indicating a rearrangement process in the initial sintering. This meant that the rates of reactions of Si_3N_4 with the liquid phase or diffusion was faster than that of particle migration. It was considered that the high viscosity of Y_2O_3–SiO_2 melts [10, 21] resulted in increased resistance to particle migration. The irregular shape and wide distribution of particle size of the starting powder may also have suppressed the migration.

TABLE I Properties of heat-treated compacts

Temperature (° C)	Time (h)	Bulk density (g cm^{-3})	Porosity (%)		Weight loss (%)	α-Phase content* (%)	Kinetic order
			Closed	Open			
1525	3	2.10	2.1	35.1	1.49	95.6	0.449
1550	3	2.21	2.1	35.0	1.67	87.7	0.467
1575	3	2.31	2.2	28.1	2.34	84.3	0.471
1600	3	2.35	2.3	27.0	3.14	77.4	0.487
1650	3	2.45	2.3	24.2	4.07	26.0	0.472
1675	2	2.49	2.5	23.0	3.74	18.3	0.477
1700	3	2.52	2.3	22.4	4.57	6.8	0.432
1725	3	2.49	2.2	23.1	5.11	5.1	0.431
1750	2	2.54	2.6	21.2	4.91	0	0.406
1850	1	2.53	2.7	21.7	6.72	0	–

*Obtained as a fractional peak intensity of α-Si_3N_4 to the sum of α-Si_3N_4 [(1 0 2) + (2 1 0) reflections] and β-Si_3N_4 [(1 0 1) + (2 1 0) reflections].

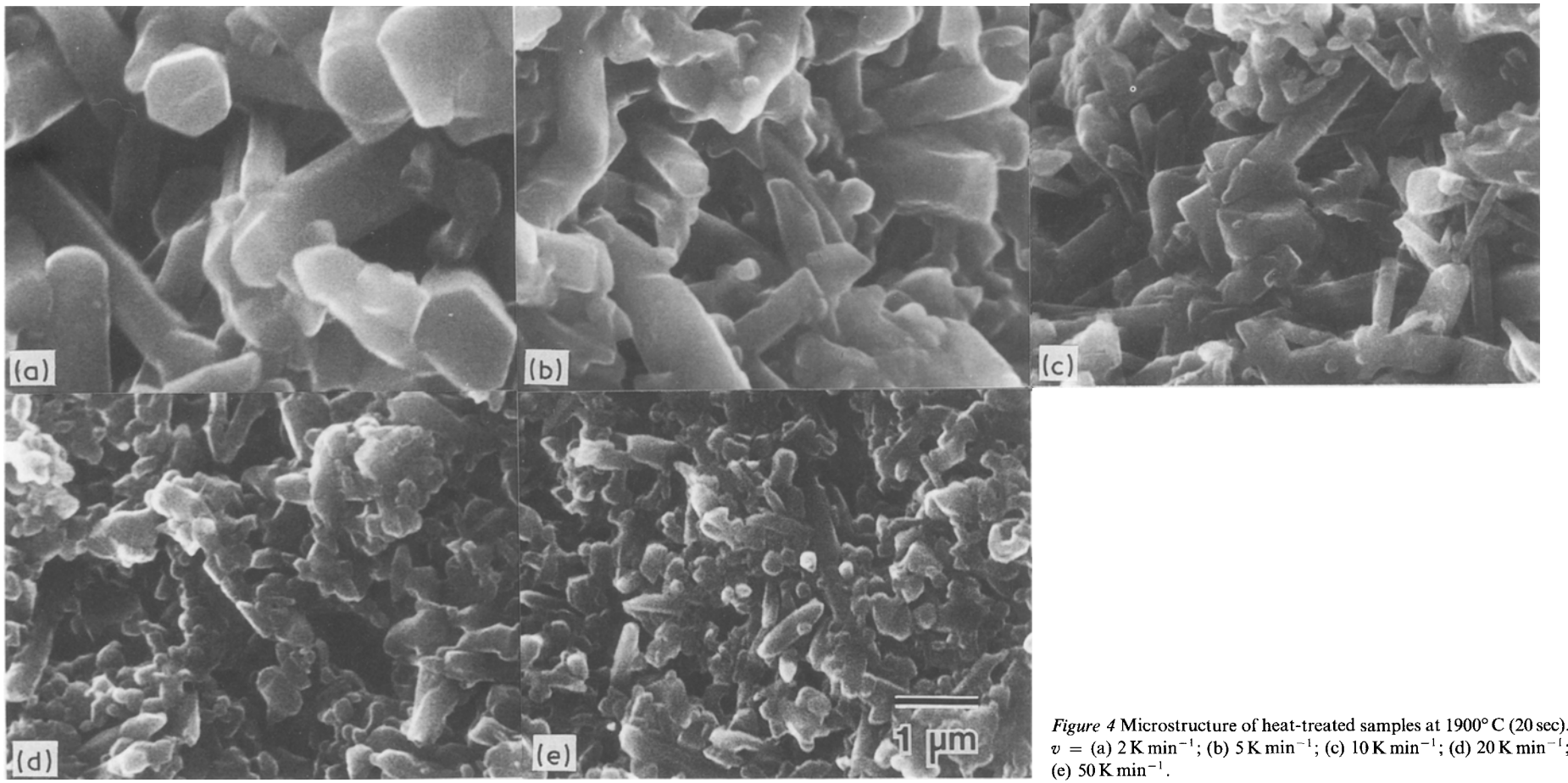

Figure 4 Microstructure of heat-treated samples at 1900° C (20 sec). v = (a) 2 K min^{-1}; (b) 5 K min^{-1}; (c) 10 K min^{-1}; (d) 20 K min^{-1}; (e) 50 K min^{-1}.

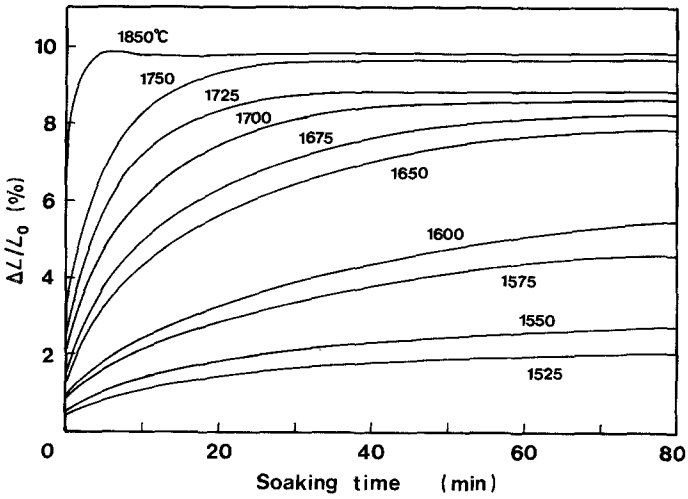

Figure 5 Isothermal shrinkage.

The kinetic order at 1525 to 1725° C indicated the boundary reaction-rate-controlling sintering. The activation energy (ΔE = 323 kJ mol^{-1}) was comparable with the Si–N bond strength (435 kJ mol^{-1}) [22] when considering the improved sinterability of the SNGX powder. The value of ΔE was greater than the activation energy of the diffusion of N atoms in SiO_2 glass (108 kJ mol^{-1}) [23]. This supported the reaction-rate-controlling mechanism, although the grain-boundary phase contained Y_2O_3. The low activation energy for diffusion did not contradict the high viscosity suppressing the rearrangement process, since the activation energy for viscous flow was usually higher than that for diffusion [24].

The kinetic order decreased below 1550° C and above 1700° C as shown in Table I. It was thought that the decrease at higher temperatures was caused by the growth of prismatic grains. Since the kinetic order for reaction-controlling densification of prismatic grains was 0.33 [18, 19]. At lower temperatures, the kinetic order may be related to the decrease of the ultrafine particles less than 0.1 μm and the change in powder shape (irregular to roundish).

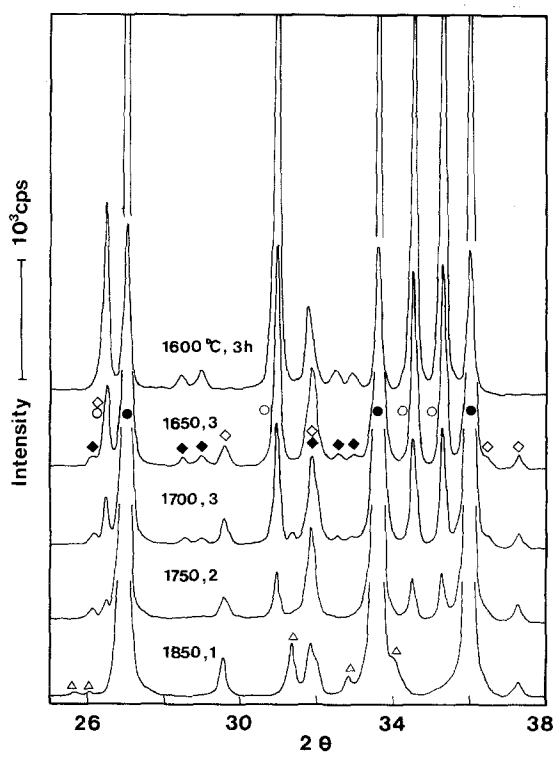

Figure 6 X-ray-diffraction patterns after isothermal dilatometry. ○, α-Si_3N_4; ●, β-Si_3N_4; ◆, $Y_2O_3 \cdot Si_3N_4$; ◇, $10Y_2O_3 \cdot 9SiO_2 \cdot Si_3N_4$; △, unknown (may be $4Y_2O_3 \cdot SiO_2 \cdot Si_3N_4$).

4.2. Characteristics of sinterable powder

The peculiarities of powders produced by nitridation-milling processes are the large specific surface area, irregularity in particle shape and the increase of the lattice strain. The large excess energy stored in powder particles is responsible for the increased reaction ability of Si_3N_4 with melts [25]. Somiya *et al.* [26] showed that the particles of the SNGX powder were covered by an amorphous surface layer, and that the lattice strain was relatively large for the SNGX powder. By electron spin resonance spectrometry (ESR) it was found that the radical concentration also increased for the SNGX powder (2.46 × 10^4 counts g^{-1}) compared with the LC-12 powder (2.02 × 10^3 counts g^{-1}). These characteristics of the SNGX powders indicate a disordered crystalline structure resulting in increased reaction ability and, therefore, a decrease of ΔE from the dissociation energy of the Si–N bond.

4.3. Grain growth

After the initial sintering, the grain growth interrupted the densification, especially when fibrous grains formed. To obtain the apparent activation energy (ΔE_a), including the influence of grain growth, the temperature dependence in Fig. 2 was replotted by the Ozawa–Doyle technique [27, 28]. In this technique, the ΔE_a was obtained by the following relation irrespective of the reaction mechansim:

$$\log v = (\text{const}) - 0.4567\, \Delta E_a/RT \qquad (2)$$

Fig. 10 shows the Ozawa–Doyle plots. Linear relations were obtained for shrinkages ranging from 4 to 7%. The ΔE_a calculated in this way was 763 to 814 kJ mol^{-1}, which was considerably higher than the ΔE for Kingery's model and the dissociation energy of the Si–N bond. The reason was that the Ozawa–Doyle plot corresponded to the Arrhenious plot of a suspected kinetic constant ($k_a = kr^{-m}$) instead of the real kinetic constant (k). The interrupting effect of densification by grain growth was estimated by using the following

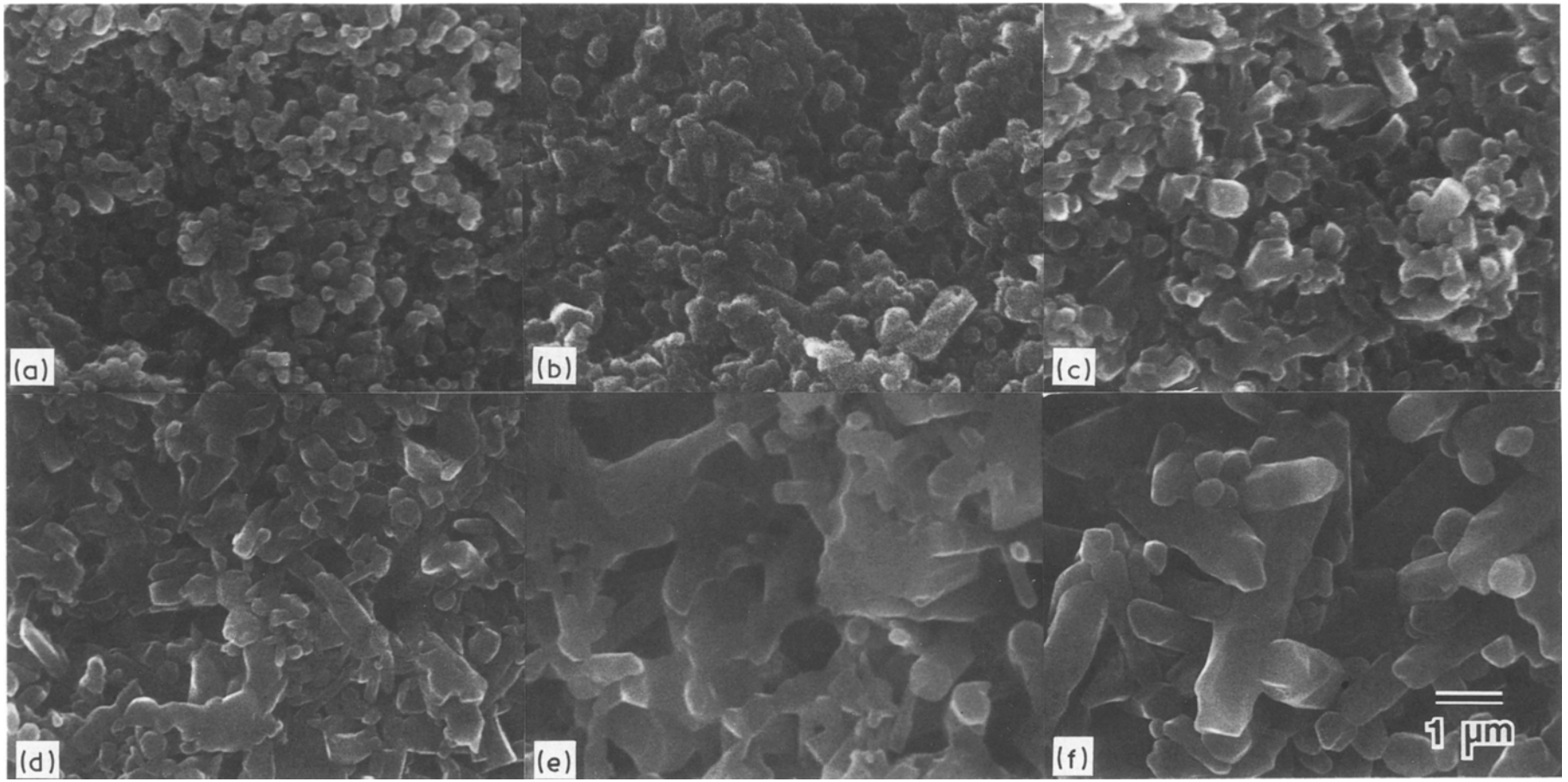

Figure 7 Microstructure of samples after isothermal dilatometry. (a) 1600° C, 3 h; (b) 1650° C, 3 h; (c) 1675° C, 2 h; (d) 1700° C, 3 h; (e) 1725° C, 3 h; (f) 1850° C, 1 h.

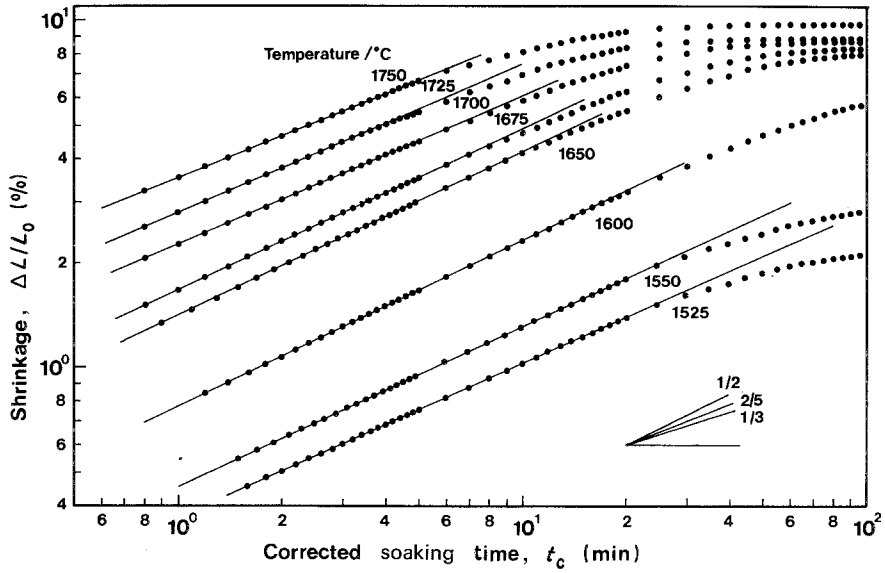

Figure 8 Log–log plots of shrinkage against corrected soaking time.

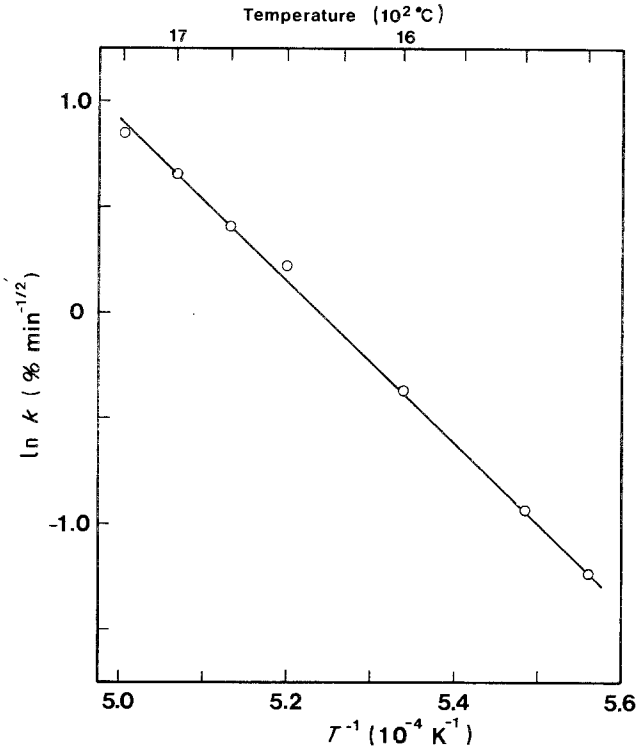

Figure 9 Arrhenius plot for the inital sintering of Y_2O_3-doped Si_3N_4.

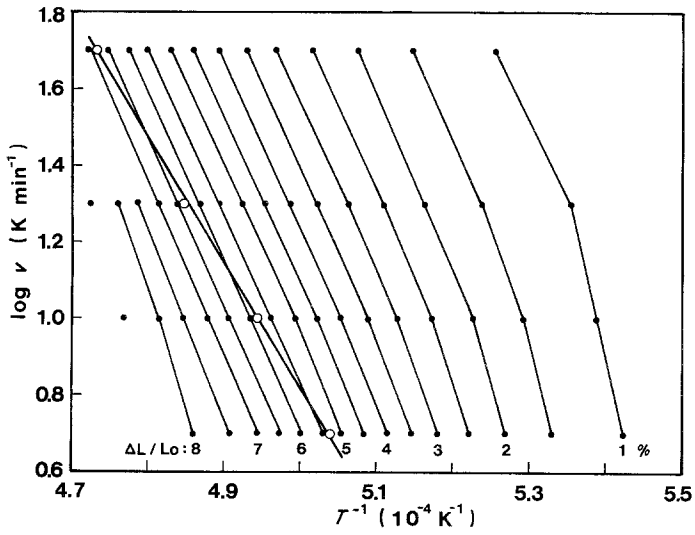

Figure 10 Ozawa–Doyle plots. Open circles indicate peak temperatures of shrinking rate.

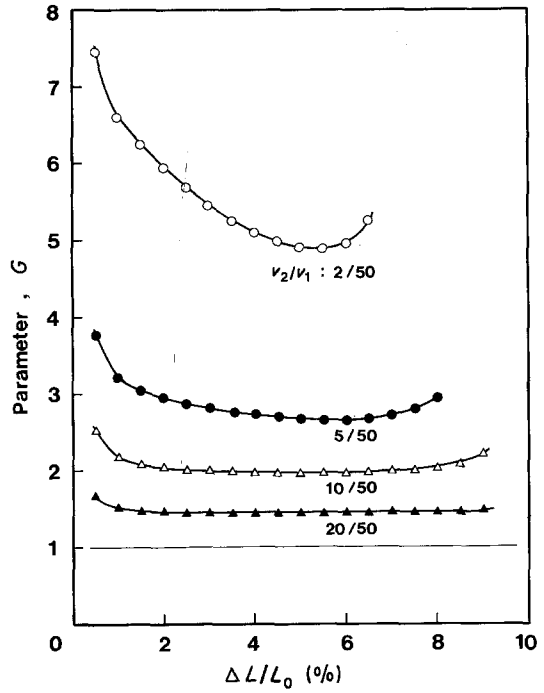

Figure 11 Parameter G indicating the interrupting effect on densification derived by the modified Ozawa–Doyle technique.

equation:

$$\Delta E_a = R\frac{\ln(k_1 r_1^{-m}) - \ln(k_2 r_2^{-m})}{T_2^{-1} - T_1^{-1}} = R\frac{\ln(k_1/k_2) + mR\ln(r_2/r_1)}{T_2^{-1} - T_1^{-1}} \quad (3)$$

By substituting the term $[R\ln(k_1/k_2)/(T_2^{-1} - T_1^{-1})]$ by ΔE, Equation 4 was obtained:

$$G = r_2/r_1 = \exp[(\Delta E_a - \Delta E)(T_2^{-1} - T_1^{-1})m^{-1}R^{-1}] \quad (4)$$

Practically, the parameter G indicates the overall interruption to densification by grain growth, change in grain shape (roundish to prismatic) and thermal decomposition between T_1 and T_2. From the Ozawa–Doyle plots, the parameter G was obtained as the difference of shrinking behaviour between two heating rates at individual shrinkages. Fig. 11 shows the parameter G at 2, 5, 10 and 20 K min^{-1} against 50 K min^{-1} as a function of shrinkage, assuming m to be unity for the boundary reaction rate controlling. The final value of the parameter G was 5.3, 2.6, 2.1 and 1.5 for 2, 5, 10 and 20 K min^{-1}, respectively. These values agreed with the ratio of grain size at v to 50 K min^{-1} in transverse direction, as shown in Fig. 4. This indicates that the influence of grain growth was greater at lower heating rates, and that the influence of the change in grain shape was almost the same for every heating rate, at least at high shrinkages. At the initial-stage sintering, the parameter was considerably higher at the low heating rate. This may be caused by the influence of the change in grain shape and the consumption of ultrafine particles.

Acknowledgements

The author thanks Dr Toriyama and Ms Matsuura of Government Industrial Research, Nagoya, for ESR measurements.

References

1. G. WÖTTING and G. ZIEGLER, in Proceedings of an International Symposium on Ceramic Components for Engines, edited by S. Somiya, E. Kanai and K. Ando (KTK Scientific, Tokyo, 1983) p. 412.
2. G. PETZOW and P. GREIL, *ibid.* p. 177.
3. G. WÖTTING, B. KANKA and G. PETZOW, "Non-oxide Technical and Engineering Ceramics", edited by S. Hampshire (Elsevier Applied Science, London, 1986) p. 83.
4. O. ABE, *Ceram. Int.* **16** (1) (1990).
5. D. W. RICHERSON, *Amer. Ceram. Soc. Bull.* **5** (1973) 560.
6. T. TABATA, *et al.*, in Proceedings of an International Symposium on Ceramic Materials and Components for Engines, edited by W. Bunk and J. Hausner (Deutsche Keram. Gesell., Lübeck-Travemunde, 1986) p. 713.
7. T. YAMADA, M. SHIMADA and M. KOIZUMI, *Amer. Ceram. Soc. Bull.* **60** (1981) 1281.
8. M. MITOMO, *J. Mater. Sci.* **11** (1976) 1103.
9. M. MITOMO and K. MIZUNO, *Yogyo-kyokai-shi* **94** (1986) 96.
10. S. HAMPSHIRE and K. H. JACK, "Special Ceramics 7", edited by D. Taylor and P. Popper (British Ceramics Society, Stoke-on-Trent, 1981) p. 37.
11. L. BOWEN, *et al.*, *J. Mater. Sci.* **13** (1978) 341.
12. D. R. MESSIER, F. L. RILEY and R. J. BROOK, *ibid.* **13** (1978) 1199.
13. R. E. LOEHMAN and D. J. ROWCLIFFE, *J. Amer. Ceram. Soc.* **63** (1980) 144.
14. C. M. HWANG and T. Y. TIEN, "Sintering '87" edited by S. Somiya *et al.* (Elsevier Applied Science, London, 1988) p. 1028.
15. R. J. WESTON and T. G. CARRUTHERS, "Ceramics for Turbines and other High-Temperature Engineering Applications", edited by D. J. Godfrey (British Ceramics Society, Stoke-on-Trent, 1973) p. 197.
16. M. J. POMEROY, B. SARUHAN and S. HAMPSHIRE, "Special Ceramics 8", edited by S. P. Howlett and D. Taylor (British Ceramics Society, Stoke-on-Trent, 1986) p. 21.
17. G. N. BABINI, A. BELLOSI and P. VINCENZINI, "Science of Ceramics 12", edited by P. Vincenzini (Ceramurgica s.r.l., Faenza, 1983) p. 169.
18. O. ABE and S. KANZAKI, *J. Ceram. Soc. Jpn.* **97** (1989) 187.
19. W. D. KINGERY, *J. Appl. Phys.* **30** (1959) 301.
20. *Idem., ibid.* **30** (1959) 307.
21. R. A. L. DREW, S. HAMPSHIRE and K. H. JACK, "Special Ceramics 7", edited by D. Taylor and P. Popper (British Ceramics Society, Stoke-on-Trent, 1981) p. 119.
22. T. L. COTTREL, "Strength of Chemical Bonds", 2nd edn (Butterworth, London, 1958) p. 216.
23. R. M. HAKIM and D. R. UHLMANN, *Phys. Chem. Glasses* **12** (1971) 132.
24. W. D. KINGERY, H. K. BOWEN and D. R. UHLMANN, "Introduction to Ceramics" 2nd edn (Wiley, New York, 1976) p. 262.
25. S. SOMIYA, *et al.*, in Proceedings of an International Symposium on Ceramic Components for Engines, edited by S. Somiya, E. Kanai and K. Ando (KTK Scientific, Tokyo, 1983) p. 442.
26. M. NAKAMURA, Y. KURANARI and Y. IMAMURA, "Silicon Nitride Ceramics", edited by S. Somiya, M. Yoshimura and M. Mitomo (Uchida Rokakudo, Tokyo, 1987) p. 27.
27. T. OZAWA, *Bull. Chem. Soc. Jpn* **38** (1965) 1881.
28. C. D. DOYLE, *Nature* **207** (1965) 290.

Received 13 March
and accepted 30 August 1989